A New Theoretical Framework for Understanding Multiscale Atmospheric Predictability

Y. Qiang Sun[1*] and Fuqing Zhang[2]

[1]*The Program in Atmospheric and Oceanic Sciences, Princeton University, Princeton, New Jersey*

[2]*Department of Meteorology and Atmospheric Science, and Center for Advanced Data Assimilation and Predictability Techniques, The Pennsylvania State University, University Park, Pennsylvania.*

*Correspondence to ys5@princeton.edu

Keywords: Numeric Weather Prediction; Predictability Limit; Error Growth Model

Early Online Release: This preliminary version has been accepted for publication in *Journal of the Atmospheric Sciences*, may be fully cited, and has been assigned DOI 10.1175/JAS-D-19-0271.1. The final typeset copyedited article will replace the EOR at the above DOI when it is published.

ABSTRACT

Here we present a new theoretical framework that connects the error growth behavior in numerical weather prediction (NWP) with the atmospheric kinetic energy spectrum. Building on previous studies, our newly proposed framework applies to the canonical observed atmospheric spectrum that has a -3 slope at synoptic scales and a -5/3 slope at smaller scales. Based on this realistic hybrid energy spectrum, our new experiment using hybrid numerical models provides reasonable estimations for the finite predictable ranges at different scales. We further derive an analytical equation that helps understand the error growth behavior. Despite its simplicity, this new analytical error growth equation is capable of capturing the results of previous comprehensive theoretical and observational studies of atmospheric predictability. The success of this new theoretical framework highlights the combined effects of quasi-two-dimensional dynamics at synoptic-scales (-3 slope) and three-dimensional turbulence-like small-scale chaotic flows (-5/3 slope) in dictating the error growth. It is proposed that this new framework could serve as a guide for understanding and estimating the predictability limit in the real world.

Accepted for publication in *Journal of the Atmospheric Sciences*. DOI 10.1175/JAS-D-19-0271.1.

\body

1. Introduction

In his pioneering work (Lorenz 1969, hereafter L69), Lorenz first showed that a flow with many length scales, like the atmosphere, might have an intrinsic finite range of predictability. Although Lorenz studied the simple 2D vorticity turbulence model in his paper, the conclusion of his study is profound and intriguing. Follow-up studies using more sophisticated models (e.g., Leith and Kraichnan 1972; Daley 1981; Foude et al. 2013; Sun and Zhang 2016; Judt 2018; Zhang et al. 2019) further supported Lorenz' results and the concept of "butterfly effect" has been widely accepted since then. Butterfly effect depicts that even the smallest unresolved errors by numerical models will propagate upscale and ruin our practical weather prediction at the synoptic-scale after a *finite* length of time (Palmer et al. 2014). Inspired by L69, estimations of this finite range of predictability has since been done extensively (e.g., Smagorinsky 1969; Lorenz 1982; Foude et al. 2013). For the synoptic weather system in mid-latitudes, more recent studies agree with Lorenz that this finite number should be around two weeks (L69; Reeves 2014; Zhang et al. 2019; Judt 2020). With this intrinsic predictability limit, current operational forecasts still have quite some room for improvement. In general, our operational weather forecast is skillful for less than 10 days in the mid-latitudes despite decades of "quiet revolution" (Bauer et al. 2015; Alley et al. 2019). To push our numerical weather prediction (NWP) skill closer to its intrinsic limit, we must understand further the error growth dynamics that limit NWP.

Over the years, conceptually and numerically simple turbulence frameworks, as used in L69, have contributed a lot to our understanding. In a turbulent fluid, the inverse cascade rate of the errors from small to large scales, which is the essence of the "butterfly effect," is noted to be intimately connected with the eddy turnover timescales that are determined by the slope of the

Accepted for publication in *Journal of the Atmospheric Sciences*. DOI 10.1175/JAS-D-19-0271.1.

background energy spectrum of the fluid. For a flow with energy spectra of power-law behavior (k^{-p}), previous studies find that if the slope $p < 3$, the eddy doubling time decreases with scale and the upscale spreading of initially small-scale error provides an intrinsical limit to the predictability of such flows; if $p \geq 3$, it is concluded that there is no such a limit (L69; Rotunno and Snyder 2008, hereafter RS2008).

Most of these studies mentioned above generally assume one single slope for the atmosphere. However, our real world is more complicated. Instead of one constant p, observational studies (e.g., Nastrom and Gage 1985) indicate that the energy spectra in the atmosphere show a distinct transition from a slope of around -3 at synoptic scales (~1000s km) to a shallower -5/3 slope at mesoscales (~100s km) in the mid-latitudes. Numerous realistic simulations, using both regional (Skamarock 2004; Waite and Snyder 2013; Sun and Zhang 2016) and global high-resolution model (Skamarock et al. 2014), also successfully reproduce the transition of the slope, consistent with the observational estimates. The mechanism(s) that determine the slopes of the kinetic energy spectra are still under debate (Charney 1971; Tulloch and Smith 2006; Callies et al. 2014). Nevertheless, according to L69 and RS2008, we would expect an intrinsic predictability limit for our atmosphere due to this shallower slope at the small-scale end of the kinetic energy spectra.

Based on the observed kinetic energy spectra, we here propose a novel and simple theoretical framework for understanding error growth from minute perturbations in the real atmosphere. This framework features a "two-stage" error growth process, which connects to the two different slopes of the observed kinetic energy spectra. Figure 1 shows a conceptual schematic for the canonical atmospheric kinetic energy spectrum and the proposed error growth behavior linked to this spectrum. An initially minute error will, in the first stage, grow much faster at small

Accepted for publication in *Journal of the Atmospheric Sciences*. DOI 10.1175/JAS-D-19-0271.1.

scales due to decreasing eddy turnover time within the -5/3 slope range. Within an inherently finite time, these small-scale errors within the -5/3 slope wavelength range will start to saturate while projecting to larger and eventually synoptic scales. In the second stage, the errors at synoptic scales (corresponding to wavelength range within the -3 slope) will grow quasi-exponentially until saturation due to near-constant eddy turnover time in this wavelength range.

With this conceptual picture, the next step is to quantify the growth of the errors under a simple analytical framework. As a tool to help our understanding of complex and chaotic nonlinear interaction, simple analytic equations have been used along with the earlier numeric studies on error growth dynamics. Lorenz (1982) showed that the growth of error variance E could be reasonably well parameterized by a simple exponential growth equation. Dalcher and Kalnay (1987) proposed a modified version based on Lorenz (1982) to describe the evolution of the error variance E

$$\frac{d}{dt}(E) = (\alpha E + S)\left(1 - \frac{E}{E_\infty}\right) \qquad (1)$$

by introducing an external error source S. This equation is adopted and widely used in studies of forecast uncertainty of operational weather prediction (e.g., Magnusson and Kallen 2013; Herrera et al. 2016; Žagar et al. 2017). However, very limited analytical work focused on the *intrinsic predictability limit* of weather systems where the external error source is eliminated.

Selz and Craig (2015) fitted the errors in their "identical twin experiments" to an analytical equation they constructed. The reasonable agreement in their study between the full-physics model and simple analytical equations implies that we may also use analytical equations to investigate the *intrinsic predictability limit.* More recently, Zhang et al. (2019) found that Eq. (1) well captured the evolution of the intrinsic error dynamics in the full-physics model. However, both studies mentioned here did not provide detailed explanations behind this consistency between the results

Accepted for publication in *Journal of the Atmospheric Sciences*. DOI 10.1175/JAS-D-19-0271.1.

of complex full-physics atmospheric models and simple analytical equations considered. This paper serves as an extension of RS2008 and Zhang et al. (2019) and aims to provide a framework that helps us further understand the connection of error growth behavior, the background kinetic energy spectrum of the real atmosphere, and the detailed analytical equation proposed. In section 2, we first revisit L69's earlier model on error growth for different kinetic energy spectrum slopes. Based on the results of the L69 model, we then propose our hybrid framework for the real atmosphere with hybrid kinetic energy spectra in section 3. A simple analytical equation is also derived in section 3 to further our understanding of the atmospheric predictability limit in the real atmosphere. A brief discussion is given in section 4.

2. Revisiting the Lorenz (1969) model

The original model of L69 was devised to study the error growth and predictability of an atmospheric-like fluid system with homogeneous isotropic turbulence using a two-dimensional vorticity (2DV) equation. In this model, Lorenz assumed power-law behavior (k^{-p}) for the basic-state kinetic energy with specific considerations dedicated to the scenarios with p = 5/3, 7/3, and 3, respectively. While these calculations are robust, it is found that the downscale energy spectral slope of a large-scale forcing for the 2DV equation is -3 (Kraichnan 1967). Given that synoptic-scale forcing is the main driver for weather systems in the mid-latitudes, the physically consistent choice for the L69 model, therefore, is p=3, which raises concerns about his results for other scenarios. The model in L69 is elegantly generalized in RS2008 to include a surface quasi-geostrophic (SQG) equation, which is known to have a -5/3 energy spectrum analogous to 3-dimensional turbulence. Our study will adopt this generalized model in RS2008 and further illustrate different error growth scenarios in 2DV (-3 slope) and SQG (-5/3 slope).

Accepted for publication in *Journal of the Atmospheric Sciences*. DOI 10.1175/JAS-D-19-0271.1.

The evolutions of the errors for the 2DV and SQG systems are detailed in L69 and RS2008. We here briefly summarize their equations as a set of second-order initial-value problems:

$$\begin{pmatrix} \frac{d^2}{dt^2}(Z_K^{2DV}) = \sum_{L=1}^{N} C_{K,L}^{2DV} Z_L^{2DV} \\ \frac{d^2}{dt^2}(Z_K^{SQG}) = \sum_{L=1}^{N} C_{K,L}^{SQG} Z_L^{SQG} \end{pmatrix} \quad (2)$$

where $C_{K,L}$ is a constant coefficient matrix derived to reflect the interactions between different length scales (K and L represent different spectral bands in the wavenumber space), N is the total number of spectral bands considered in the model[1]. The structure and amplitude of $C_{K,L}$ is determined by the dynamic model and, more importantly, by the background kinetic energy spectrum of the fluids (refer to L69 and RS2008). Z_K^{2DV} and Z_K^{SQG} are the ensemble means of the perturbation kinetic energy (error fields) for the 2DV and SQG equations, respectively, integrated over any given spectral band K. For each spectral band K, errors with different length scales (spectral bands) also contribute to the evolution of Z_K^{2DV} and Z_K^{SQG}. In addition, both L69 and RS2008 also introduce nonlinear saturation treatment to their equations by directly letting Z_K fixed at its corresponding background kinetic energy X_K if $Z_K(t) \geq X_K$ in the course of the integration. This treatment makes no change to the growth rate of Z_K until it reaches saturation. To better describe the gradual decrease in the growth rate of Z_K as it approaches saturation, Durran and Gingrich (2014) introduces one additional term $\left(1 - {Z_K}/{X_K}\right)$ to force the time tendencies of the Z_K smoothly asymptote to zero as Z_K approaches X_K. The same nonlinear treatment as Durran and Gingrich (2014) is applied to our numerical model (Appendix A) to make it more realistic.

[1] Adjacent spectral bands are differed by a constant resolution factor ρ ($\rho = \sqrt{2}$ in this study). Assuming the length scales for all N spectral bands are $D_0, D_1, \ldots D_{N-1}$, then we have $D_0 = \rho^K D_K$ for each spectral band K.

Accepted for publication in *Journal of the Atmospheric Sciences*. DOI 10.1175/JAS-D-19-0271.1.

Despite similar forms in Eq. (2), very different error evolutions are found between the 2DV (-3 slope) case versus the SQG (-5/3 slope) case, which are rooted in their striking differences in $C_{K,L}$ (see Table 1 and Table 3 in RS2008) and the corresponding basic-state spectra. Through directly comparing their results with L69, RS2008 concluded that the basic-state energy spectrum was the determining factor in the error-energy evolution. They showed that a -5/3 spectrum would lead to limited predictability under varying dynamical models, while a -3 spectrum may have unlimited predictability when the initial perturbation becomes infinitesimally small.

2.a Error growth for the 2DV case (-3 slope)

Figure 2 depicts the error growth in different experiments using the 2DV equation under different initial condition errors. For each experiment, the initial error distribution is set so that the error field is limited to the small scales only. No initial error is added to the spectral bands that have larger length scales than the cutoff spectral band *K* (cutoff *K* in Fig. 2a)[2]. For length scales equal to or smaller than spectral band *K,* their initial error amplitudes are set to their saturation values. Increased *K* means that the initial error is pushed to smaller scales, and thus its amplitude is exponentially reduced. We can find that, as the cutoff *K* increases (initial error reduces exponentially), the time needed for the error to saturate at large scales increases linearly (Fig. 2b). Therefore, if we could keep reducing the initial error to smaller and smaller scales, we could keep increasing the error saturation time at large scales without any limitation.

This linearity in Fig. 2b also implies that a similar amount of additional predictable time can be gained each time we increase *K* and therefore limit the initial condition errors to a smaller scale. In other words, error growth at different length scales can be characterized by a single growth

[2] Given the power-law distribution of the base spectrum, the total initial error will decrease exponentially when we linearly increase *K*.

Accepted for publication in *Journal of the Atmospheric Sciences*. DOI 10.1175/JAS-D-19-0271.1.

rate in the 2DV case. Indeed, this uniform error growth rate agrees well with the turbulence assumption for a flow with a -3 spectrum. More specifically, if $\boldsymbol{A}$ is a measure of the amplitude of the total error energy, then the evolution of $\boldsymbol{A}(t)$ could be written as

$$\frac{d}{dt}\boldsymbol{A} = \alpha \boldsymbol{A}$$

assuming α is the error growth rate. The error doubling time τ_D can be then calculated to be $\tau_D = \frac{\ln(2)}{\alpha}$, inversely proportional to the error growth rate α. From the turbulence perspective, the scale-dependent error doubling time $\tau_D(k)$ is comparable to the eddy turnover time τ_k. τ_k is a characteristic timescale that is defined as the time taken for a parcel with velocity v_k to move a distance $1/k$, v_k being the velocity associated with the (inverse) scale k. τ_k can be estimated from the spectral energy density $E(k)$ (e.g., see Vallis 2006 page 349),

$$\tau_k \sim \sqrt{\frac{k^{-3}}{E(k)}}, \quad \tau_D(k) = O(1)\,\tau_k = D\sqrt{\frac{k^{-3}}{E(k)}} \qquad (3)$$

where D is a constant on the order of unity. Therefore, we have,

$$\alpha = \frac{ln2}{\tau_D(k)} = \frac{ln2}{D}\sqrt{\frac{E(k)}{k^{-3}}} \qquad (4)$$

which means that the error growth rate is constant for the 2DV case since $E(k) \propto k^{-3}$. Given this constant α, the evolution of the total error energy in the 2DV case Z_{total}^{2DV} can be simplified as

$$\frac{d}{dt}(Z_{total}^{2DV}) = \alpha Z_{total}^{2DV} \qquad (5)$$

To include the error saturation effect at later times, we could also add an additional term as in Durran and Gingrich (2014) to force the time tendency of Z_{total}^{2DV} to decrease smoothly to 0 as Z_{total}^{2DV} approaches its saturation threshold Z_{sat}^{2DV}. With this adjustment, Eq. (5) becomes

Accepted for publication in *Journal of the Atmospheric Sciences*. DOI 10.1175/JAS-D-19-0271.1.

$$\frac{d}{dt}(Z_{total}^{2DV}) = \alpha Z_{total}^{2DV}\left(1 - \frac{Z_{total}^{2DV}}{Z_{sat}^{2DV}}\right) \qquad (6)$$

While this additional term is ad hoc, Eq. 6) captures the error growth behavior reasonably well (Fig. 2c).

2.b Error growth for the SQG case (-5/3 slope)

For the SQG scenario, with a -5/3 slope, the eddy turnover time in Eq. (3) will decrease exponentially with decreasing length scales. Hence, the gain in extra forecast lead time through further limiting the initial error to smaller scales will also become exponentially smaller. More specifically, by increasing cutoff K in the experiments (e.g., for experiments of K=12 and K=13 in Fig.3a), the additional time we gain is simply the time it takes for the initial errors to propagate back and saturate larger scales (e.g., upscale growth from K=13 to K=12), which is on the order of the eddy turnover time at that scale ($\tau_{K=12}$). Given exponentially decreasing eddy turnover time under a -5/3 slope, Fig. 3b shows that the error saturation time at large scales can be extended at most by a few turnover cycles of the current smallest resolved scale, and it will eventually approach a near-constant value when the initial condition error approaches zero.

This limited predictability for the SQG (-5/3 slope) case could also be explained according to the turbulence energy cascade theory. After a finite time (on the order of eddy turnover time of the large-scale end if estimated using the turbulence assumption, more on this in Appendix B), errors will saturate no matter how small the initial error is. What we care about the most here is the characteristic finite timescale needed for the errors to saturate. For simplicity, we could write the error growth equation to be

$$\frac{d}{dt}(Z_{total}^{SQG}) = \gamma \qquad (7)$$

Accepted for publication in *Journal of the Atmospheric Sciences*. DOI 10.1175/JAS-D-19-0271.1.

where Z_{total}^{SQG} is the total error for the SQG scenario. Assuming the saturation value of the total error for the SQG case is Z_{sat}^{SQG}, then the time needed for the error to saturate, according to Eq. (7), is simply Z_{sat}^{SQG}/γ. γ is the linear error growth rate that may vary with different base-state kinetic energy spectra and different initial condition errors. We acknowledge this linear error growth is not very realistic or physical. Yet, it is very simple and provides an estimation for the error saturation time if we know the value of γ. Similar to Eq. (6) , we need to add a saturation term $\left(1-\frac{Z_{total}^{SQG}}{Z_{sat}^{SQG}}\right)$ to represent the saturation effect when Z_{total}^{SQG} approaches its saturation value Z_{sat}^{SQG}. Eq. (7) then becomes

$$\frac{d}{dt}\left(Z_{total}^{SQG}\right) = \gamma\left(1-\frac{Z_{total}^{SQG}}{Z_{sat}^{SQG}}\right) \qquad (8)$$

Figure 3c further verifies that Eq. (8), which simply provides an estimation for the error saturation time, might not be a bad approximation for the original numerical solution of SQG-like error dynamics in Eq. (2).

Compared to Eqs. (2), Eq. (6) and Eq. (8) are more simplified with known analytical solutions that are much easier to understand. Moreover, we can estimate the parameters in both analytical error growth models from their respective basic-state spectrum. For example, α can be estimated from Eq. (4), whereas γ is related to the eddy turnover time at the large-scale end of the -5/3 spectrum (more details will be discussed later). Next, we will combine and extend these simple analytical formulas to further explain the complex multiscale predictability of the real atmosphere.

3. The hybrid framework

3.a The hybrid L69 model

Accepted for publication in *Journal of the Atmospheric Sciences*. DOI 10.1175/JAS-D-19-0271.1.

In the real atmosphere, different from either 2DV or SQG, the observed kinetic energy spectra in the upper troposphere in the mid-latitudes usually consist of a -3 spectrum at the synoptic scales and a -5/3 spectrum at meso- and smaller scales (Nastrom and Gage 1985). Therefore, the error growth representative of the observed atmospheric energy spectra would have simultaneous contributions from both the 2DV-like spectrum at synoptic scales and the SQG-like spectrum at smaller scales. The ensemble means of the total error for any spectral bank K can then be written as

$$\frac{d^2}{dt^2}\left(Z_K^{total}\right) = \frac{d^2}{dt^2}\left(Z_K^{SQG} + Z_K^{2DV}\right) \qquad (9)$$

which is a combination of the two ODEs in Eq. (2) and could be solved numerically as before. We should note here that the nonlinear saturation adjustment, as in Durran and Gingrich (2014), is also added to Eq. 9) when solving this equation. More details on this can be found in Appendix A. Due to this additional *nonlinear* saturation effect, the hybrid model of Eq. (9) cannot be linearly decoupled as the summation of a solution to the SQG-like system and a solution to the 2DV-like system.

Figure 4 shows an example of the error evolution solved from Eq. (9), with the saturation terms included. To solve this hybrid model, we first construct a hybrid basic-state energy spectrum similar to the observed spectrum[3] and the $C_{K,L}^{2DV}$ and $C_{K,L}^{SQG}$ are then computed based on the respective -3 and -5/3 parts of the kinetic energy spectrum (see Appendix A for more details). Consistent with our schematic shown in Fig. 1, we can find that the errors first grow at small scales that are dominated by the -5/3 slope. These errors at the small scales then start to saturate at increasingly larger scales, and the total error growth will come predominantly from the -3 slope

[3] The observed spectrum transition happens at ~400km in the mid-latitudes, corresponding to zonal wavenumber ~70.

Accepted for publication in *Journal of the Atmospheric Sciences*. DOI 10.1175/JAS-D-19-0271.1.

247 part of the kinetic energy spectrum after the smaller-scale errors saturate. Moreover, given that
248 the evolution of small-scale errors is dominated by the SQG-like spectra, further reducing initial
249 errors to infinitesimal scales does not help extend the predictability limit.
250
251 ***3.b The analytical equation***
252 To derive an analytical expression for error growth under the observed hybrid spectra, we
253 first separate the total errors $\mathcal{E}_t$ into two parts according to different length scales. The total errors
254 $\mathcal{E}_t = \mathcal{E}_{-\frac{5}{3}} + \mathcal{E}_{-3}$. Here $\mathcal{E}_{-\frac{5}{3}}$ represents the meso-small scales errors in the -5/3 slope regime, $\mathcal{E}_{-3}$
255 represents the synoptic-scale errors in the -3 slope regime,
256 Given the decreasing eddy turnover time within the -5/3 slope regime, the meso-small
257 scales errors $\mathcal{E}_{-\frac{5}{3}}$ feature SQG-like upscale growth. At the same time, this upscale growth process
258 would transfer a small portion of these smaller-scale errors into the synoptic scales due to cross-
259 scale nonlinear interaction. While the physical mechanisms of the upscale error propagation in the
260 real atmosphere are still under investigation (Zhang et al. 2007; Bierdel et al. 2018), this effect is
261 included in $C_{K,L}$ terms in the numerical solution. In light of Eq. (7), the evolution of small-scale
262 errors $\mathcal{E}_{-\frac{5}{3}}$ could then be simplified as

263 $$\frac{d}{dt}\left(\mathcal{E}_{-\frac{5}{3}}\right) = \gamma' - \Gamma\left(\mathcal{E}_{-\frac{5}{3}}, \mathcal{E}_{-3}\right) \quad (10)$$

264 where γ' represents the SQG-like upscale error growth as in Eq. (7) and $\Gamma\left(\mathcal{E}_{-\frac{5}{3}}, \mathcal{E}_{-3}\right)$ here
265 represents the energy that is transited to the synoptic scales through interactions between the -3
266 slope and the -5/3 slope. An additional nonlinear saturation treatment as in Eq. (8) will be
267 introduced later. Given that the -3 slope regime has much weaker cross-scale interaction compared
268 to the -5/3 slope regime, it is reasonable that the small-scale errors are dominated by the SQG-like

Accepted for publication in *Journal of the Atmospheric Sciences*. DOI 10.1175/JAS-D-19-0271.1.

error growth associated with the -5/3 slope only, which implies that the γ' term shall dominate the $\Gamma\left(\mathcal{E}_{-\frac{5}{3}}, \mathcal{E}_{-3}\right)$ term in Eq. (10). The numerical solution in Fig. 4 also suggests that the initial growth of the errors under a hybrid spectrum is mostly on the small-scale end. Therefore, assuming $\mathcal{E}_{-\frac{5}{3}}^{sat}$ is the saturation error for the -5/3 slope regime, we can neglect the $\Gamma\left(\mathcal{E}_{-\frac{5}{3}}, \mathcal{E}_{-3}\right)$ term here and use $\mathcal{E}_{-\frac{5}{3}}^{sat} \Big/ \gamma'$ as a simple estimate of the characteristic time needed for the small scale errors $\mathcal{E}_{-\frac{5}{3}}$ to saturate.

On the other hand, the errors at the synoptic scales will have both the 2DV-like exponential growth and the contributions from smaller scales. In light of Eq. (5) and the subtraction of the $\Gamma\left(\mathcal{E}_{-\frac{5}{3}}, \mathcal{E}_{-3}\right)$ term in Eq. (10), the evolution of $\mathcal{E}_{-3}$ could also be approximately written as:

$$\frac{d}{dt}(\mathcal{E}_{-3}) = \alpha\mathcal{E}_{-3} + \Gamma\left(\mathcal{E}_{-\frac{5}{3}}, \mathcal{E}_{-3}\right) \quad (11)$$

where α is the corresponding error growth rate for the synoptic scales.

Combining Eq. (10) and Eq. (11), we can write the evolution for the total errors $\mathcal{E}_t$,

$$\frac{d}{dt}(\mathcal{E}_t) = \frac{d}{dt}\left(\mathcal{E}_{-\frac{5}{3}} + \mathcal{E}_{-3}\right) = \alpha\mathcal{E}_{-3} + \gamma' \quad (12)$$

Again, we can add $\left(1 - \frac{\mathcal{E}_t}{\mathcal{E}_t^{sat}}\right)$ term to describe the saturation of $\mathcal{E}_t$, similar to Eq. (6) and Eq. (8). The equation then becomes

$$\frac{d}{dt}(\mathcal{E}_t) = \left(\alpha\mathcal{E}_{-3} + \gamma'\right)\left(1 - \frac{\mathcal{E}_t}{\mathcal{E}_t^{sat}}\right) \quad (13)$$

Note that this equation is very similar to Eq. (1) that is used in Zhang et al. (2019) and earlier studies (e.g., Dalcher and Kalnay 1987; Magnusson and Källén 2013). The only difference

Accepted for publication in *Journal of the Atmospheric Sciences*. DOI 10.1175/JAS-D-19-0271.1.

between Eq. (13) and Eq. (1) is that $\mathcal{E}_{-3}$ in Eq. (13) is replaced with total error variance $\mathcal{E}_t$ (E in Eq. (1)), which allows us to provide an analytical solution to the total error $\mathcal{E}_t$. Moreover, this change is a valid approximation of Eq. (13). When $\mathcal{E}_t$ is small, the growth of the errors is dominated by SQG-like upscale process (the γ' term in Eq. (13) is much larger than $\alpha\mathcal{E}_t$ or $\alpha\mathcal{E}_{-3}$). Changing $\mathcal{E}_{-3}$ to $\mathcal{E}_t$ only has minor impacts on the results. When $\mathcal{E}_t$ becomes larger, then the 2DV-like growth dominates, $\mathcal{E}_{-3}$ approximates to the value of $\mathcal{E}_t$ due to the relatively small saturation value of $\mathcal{E}_{-\frac{5}{3}}^{sat}$. Therefore, we could approximately replace $\mathcal{E}_{-3}$ with $\mathcal{E}_t$ and define $\varepsilon = \mathcal{E}_t/\mathcal{E}_t^{sat}$, then Eq. (13) becomes

$$\frac{d\varepsilon(t)}{dt} = (\alpha\varepsilon(t) + \beta)\big(1 - \varepsilon(t)\big) \qquad (14)$$

where ε(t) is the normalized error. ε=1 means error reaches a maximum or becomes saturated. α is the error growth rate and $\beta = {\gamma'}/{\mathcal{E}_t^{sat}}$. Figure 4b shows the evolution of normalized total errors derived by numerically solving saturation adjusted Eq. (9) versus the fitted curve using the analytical solution derived from Eq. (14). Both solutions agree with each other well. As mentioned earlier, Eq. (14) was also proposed in earlier studies and shown to be useful. Through simple derivation and approximation, our contribution here focuses on directly linking β with the intrinsic upscale error growth (associated with the shallower -5/3 spectrum) under a nearly perfect model and nearly perfect initial condition scenario.

Indeed, similar to α, the parameter β could also be estimated directly from the kinetic energy spectrum $E(k)$ under our framework. We use β to represent upscale error growth processes from small convective scales to mesoscales within the -5/3 slope range (stage 1 of Fig. 1). After some time t_{kt}, the mesoscale error will start to saturate, and the large-scale quasi-exponential error growth starts to dominate. In Eq. (14), the transition happens when $\alpha\varepsilon(t_{kt}) = \beta$, which implies

Accepted for publication in *Journal of the Atmospheric Sciences*. DOI 10.1175/JAS-D-19-0271.1.

$$\varepsilon(t_{kt}) = \frac{\beta}{\alpha} \qquad (15)$$

Before t_{kt}, we have

$$\beta \sim \beta\big(1-\varepsilon(t)\big) < \frac{d\varepsilon(t)}{dt} < \alpha\varepsilon(t) + \beta < 2\beta \qquad (when\ t < t_{kt}, \varepsilon(t)\ is\ small\ ) \qquad (16)$$

or,

$$\frac{d\varepsilon(t)}{dt} \sim \beta, \qquad (when\ t < t_{kt}) \qquad (17)$$

Combining Eqs. (15) and (17), we have,

$$t_{kt} = {\varepsilon(t_{kt})}\Big/{\frac{d\varepsilon(t)}{dt}} \sim \left({\left(\frac{\beta}{\alpha}\right)}\Big/{\beta}\right) = \frac{1}{\alpha} \qquad (18)$$

Recall Eqs. (7) and (10), the characteristic time needed for the smaller-scale errors $\mathcal{E}_{-\frac{5}{3}}$ to saturate could also be estimated to be

$$t_{kt} \sim \frac{\mathcal{E}_{-\frac{5}{3}}^{sat}}{\gamma'} = \frac{\mathcal{E}_{-\frac{5}{3}}^{sat}}{\beta\, \mathcal{E}_t^{sat}} \qquad (19)$$

Combining Eq. (18) and Eq. (19), we get

$$\frac{1}{\alpha} \sim \frac{\mathcal{E}_{-\frac{5}{3}}^{sat}}{\beta\, \mathcal{E}_t^{sat}}, \qquad or \qquad \frac{\beta}{\alpha} \sim \frac{\mathcal{E}_{-\frac{5}{3}}^{sat}}{\mathcal{E}_t^{sat}} \qquad (20)$$

where

$$\frac{\mathcal{E}_{-\frac{5}{3}}^{sat}}{\mathcal{E}_t^{sat}} = \frac{saturated\ kinetic\ energy\ of\ \ k^{-\frac{5}{3}}\ regime}{total\ kinetic\ energy}$$

If the kinetic energy spectrum $E(k)$ is known and fits the canonical atmospheric kinetic energy spectrum in Fig. 1, then we could define k_t as the wavenumber of the transition scale of the kinetic energy spectrum. For any wavenumber k that is greater than k_t but smaller than k_s (the

Accepted for publication in *Journal of the Atmospheric Sciences*. DOI 10.1175/JAS-D-19-0271.1.

wavenumber at the smallest scale resolved), $E(k)$ lies in the -5/3 regime. The kinetic energy in the -5/3 slope regime can then be written as $\int_{k_t}^{k_s} E(k)\,dk$. Similarly, we can also write the total kinetic energy as the sum of the kinetic energy in the -3 slope regime and the kinetic energy in the -5/3 slope regime, hence

$$\mathcal{E}_t^{sat} = \int_{k_l}^{k_t} E(k)\,dk + \int_{k_t}^{k_s} E(k)\,dk = \int_{k_l}^{k_s} E(k)\,dk \quad (21)$$

where k_l is the wavenumber at the largest scale that a -3 slope might hold. Therefore, we have

$$\frac{\beta}{\alpha} \sim \frac{\mathcal{E}_{-\frac{5}{3}}^{sat}}{\mathcal{E}_t^{sat}} = \frac{\int_{k_t}^{k_s} E(k)\,dk}{\int_{k_l}^{k_s} E(k)\,dk} \quad (22)$$

Another easy way to estimate the value of β is by utilizing the schematic shown in Fig. 1. At transition time t_{kt}, the small-scale errors in the -5/3 regime start to saturate, and the large-scale errors in the -3 regime are still negligible. Therefore the normalized error could be estimated to be $\frac{\mathcal{E}_{-\frac{5}{3}}^{sat}}{\mathcal{E}_t^{sat}}$. Combining this with Eq. (15), once again, we have Eq. (22).

In light of Eq. (4) and Eq. (22), if the canonical atmospheric kinetic energy spectrum $E(k)$ is known to us, then we can directly estimate the error growth behavior of the system using the analytical Eq. (14) proposed above, the parameter of this analytical equation can be calculated as follows:

$$\alpha = \frac{ln2}{D}\sqrt{\frac{E(k)_{synoptic\ scale}}{k^{-3}}}, and\ \frac{\beta}{\alpha} = \frac{\int_{k_t}^{k_s} E(k)\,dk}{\int_{k_l}^{k_s} E(k)\,dk} \quad (23)$$

To sum up, this simple analytical framework that we show is consistent with the error growth scenario described in Fig. 1. This framework is also well connected to the background

Accepted for publication in *Journal of the Atmospheric Sciences*. DOI 10.1175/JAS-D-19-0271.1.

kinetic energy spectrum. All parameters in the analytical error growth model can be directly estimated from the energy spectrum of the background flow (Eq. 23).

3.c Verification and predictability limits

It is natural to ask how well our proposed hybrid framework applies to the real atmosphere. For a more direct comparison, simple dimensional results are used here. The largest length scale L_0 (corresponding to wavenumber 1) is chosen to be the circumference of a latitudinal cycle at the mid-latitude (~30000 km). The total kinetic energy of the background flow E is estimated to be 150 m^{-2} s^{-2}, as in L69[4]. The units of distance and time are then $L^* = {L_0}/{2\pi}$ and $T^* = {L^*}/{\sqrt{E}} \sim 4.25\ day$, respectively. Therefore $t = 1$ in the equation represents 4.25 days in the real atmosphere.

Table 1 shows the predictability limit derived from Eq. (9) of our hybrid framework and the results from L69. For L69, the predictability limit is simply the time when $Z_K(t) = X_K$. We use a 99% threshold for the calculation of the saturation time in our hybrid model under the Durran and Gingrich (2014) adjustment. Clearly, the predictability limits in our hybrid framework are much longer than L69. The reasons for this are twofold. On the one hand, L69 used a -5/3 slope across all the scales. By switching to the -3 slope at the synoptic scales as in the real atmosphere, our hybrid framework has less energy at smaller scales (consistent with observations), which leads to longer eddy turnover time, lower error growth rate, and hence longer predictability limit. On the other hand, the saturation approach we adopted from Durran and Gingrich (2014) will slow down

[4] L69 use 148 m^{-2} s^{-2} for total energy. Density weighted total energy from reanalysis data give a strong seasonal variation, ranging from less than 100 m^{-2} s^{-2} in the summer and more than 200 m^{-2} s^{-2} in the winter.

Accepted for publication in *Journal of the Atmospheric Sciences*. DOI 10.1175/JAS-D-19-0271.1.

the error growth rate as the errors approach their saturation threshold, which also will extend the predictability limit.

What is more intriguing is that the proposed hybrid framework shows an approximate two-week limit for the synoptic scales at ~ 5000km. This limit agrees with our current understanding. The same two-week limit for day-to-day weather predictability was first proposed by Lorenz in his early studies by analyzing the operational model products (Lorenz 1973, 1984; Reeves 2014). This limit is also found in today's most sophisticated numerical models (Foude et al. 2013; Judt 2018; Zhang et al. 2019). Moreover, the fitted α and β in Fig. 4b also agree well with the number estimated using full-physics convection-permitting global simulation (Fig. 3 in Zhang et al. 2019). While all the predicted limits will vary proportionally with slightly different dimensional analysis (due to uncertainty in total kinetic energy *E,* for example), the ratio between the saturation times for different length scales will hold under dimensional process. Assuming this 2-week limit for the synoptic weather, then we learn from table 1 that the predictability limit for motions at ~1000 km is ~7 days, the predictability limit for ~500 km is ~ 5 days, and ~2 days for 100 km. All these numbers are generally consistent with the findings derived from complex, state-of-the-science modeling experiments in Zhang et al. (2019).

As we have mentioned before, we could also estimate the value of α and β from the kinetic energy spectrum directly. Utilizing the airplane data (Marenco et al. 2018), the observed atmospheric spectrum was fitted to a functional form in Lindborg (1999),

$$E(k) = d_1 k^{-\frac{5}{3}} + d_2 k^{-3} \qquad (24)$$

where $d_1 = 9.1 \times 10^{-4}, d_2 = 3 \times 10^{-10}$. Note $E(k)$ has units of $\mathrm{m}^3 \cdot s^{-2}$, k has units of m^{-1}. Therefore d_1 has units of $\mathrm{m}^{4/3} \cdot s^{-2}$, d_2 has units of s^{-2}. The first term of Eq. (24) describes the shallower -5/3 wavelength range of the observed kinetic energy spectrum, while the second term

Accepted for publication in *Journal of the Atmospheric Sciences*. DOI 10.1175/JAS-D-19-0271.1.

of Eq. (24) fits the synoptic -3 slope wavelength range. Figure 7 of Lindborg (1999) shows that this functional form of Eq. (24) works well for horizontal scales smaller than 1000 km when compared with the airplane observation data. Substituting Eq. (24) into Eq. (3) and assuming D equals 1.0, we find that the eddy turnover time for the synoptic-scale regime is around 16 hours that is independent of the wavenumber k. The value of α is then estimated to be around $\frac{1}{1\ day}$ according to Eq. (23). Moreover, from Eq. (24) we can also tell the transition scale $k_t \sim {}^{2\pi}/_{400km}$ (considering $d_1 k_t^{-\frac{5}{3}} = d_2 k_t^{-3}$). Assuming $k_l \sim {}^{2\pi}/_{10000km}$, $k_s \sim {}^{2\pi}/_{1km}$, then $\frac{\beta}{\alpha}$ can also be estimated to be on the order of 1/100 using Eq. (23). Hence, for the midlatitudes, an estimate of α and β from the energy spectrum can be given here,

$$\alpha \sim \frac{1}{1\ day}, \qquad \frac{\beta}{\alpha} \sim \frac{1}{100}, \qquad \beta \sim \frac{\alpha}{100} \sim \frac{1}{15\ min} \tag{25}$$

These numbers, again, approximately match what we found in Fig. 4b and in earlier works done using full-physics models (Zhang et al. 2007, 2019).

4. Discussion

This proposed hybrid framework extends and complements earlier studies done by L69 and RS2008. By considering both the synoptic-scale 2DV-like dynamics (-3 slope) and the SQG-like motions (-5/3 slope) at smaller scales, our framework provides an improved understanding of the real atmosphere. The dimensional results also confirm that this hybrid framework gives more realistic estimations of the predictability limit compared to L69. To better understand the error growth process, we further derive a simple analytical equation for the evolution of the total error fields, which seems to work well with the idealized and full-physics simulation (Zhang et al. 2019).

Accepted for publication in *Journal of the Atmospheric Sciences*. DOI 10.1175/JAS-D-19-0271.1.

We note here the canonical atmospheric kinetic energy spectra shown in Fig. 1 is really an idealization of the aircraft observations, which mainly reflect the upper levels in the mid-latitudes. This canonical structure, however, is not always observed in the real atmosphere, which varies with different seasons, latitudes, and height levels. While the -3 slope and -5/3 slope are strictly assumed when building our new hybrid framework, it is easy to find that both numbers are likely not strictly required. On the smaller-scale end, the predictability limit, according to L69, will be limited as long as the slope is shallower than -3. L69 also showed that a -7/3 slope produced very close estimates of the predictability limit to the -5/3 scenario. Switching the slope of the small-scale spectrum from -5/3 to -7/3 or -2 in our hybrid model also has minor effects on the results and the predictability limits at large synoptic scales (not shown). The -3 slope for the synoptic scales plays a more significant role in determining the predictability limits in the sense that a steeper slope (e.g., -4 slope) will lead to longer predictability limits at the largest synoptic scales. As the 2DV and SQG dynamics do not support slopes other than -3 and -5/3, the experimental results of changing the slopes to different numbers based on the 2DV/SQG system are therefore less convincing. Yet, based on the eddy turnover time argument, a slightly different slope shall not change the general picture ("two-stage" error growth process) shown in Fig. 1.

We shall acknowledge the fact that this newly proposed framework is based on L69. Therefore all the assumptions made in L69 are still used in our current framework, which may pose limitations to the application of the framework. First, the statistical assumptions made in L69, such as homogeneity and isotropy, are not strictly valid for the real atmosphere. These assumptions do not allow any climatological mean motions and properties. It is also well known that systems like mountains and clouds are not randomly distributed. This heterogeneity could also be found in the kinetic energy spectrum of the real atmosphere. A recent global high-resolution simulation

Accepted for publication in *Journal of the Atmospheric Sciences*. DOI 10.1175/JAS-D-19-0271.1.

shows that the kinetic energy spectrum of the tropical region is different from the canonical spectrum shown in Fig. 1 (Judt 2020), indicating that the tropics may have very different error growth behavior than the mid-latitudes. Second, the specific dynamical equations adopted are also not strictly accurate for the real atmosphere. The two-dimensional vorticity equation is, at best, a very crude approximation for the large-scale dynamics. There is also no evidence showing that the small-scale dynamics could be described using surface quasi-geostrophic equations. Nonetheless, RS2008 has shown that, from the perspective of error growth, the kinetic energy spectrum slope might be more important compared to the dynamical equations used. The reason we choose these equations is also that their spectra are defensible on physical grounds so that we can combine them to construct a hybrid spectrum that is consistent with observational and full-physics modeling studies. With a realistic transition of the kinetic energy spectrum slope, we expect that our hybrid framework would capture the key components of the error growth behavior.

We also note here that we were not able to prove the causality between the kinetic energy spectrum and the error growth behavior in our framework. There are distinct differences between correlation and causation. It is also possible that the same physical processes/mechanisms lead to both the transition of the slopes and the error growth behavior simultaneously. For example, it has been hypothesized that moist convection and gravity waves generated by that might be responsible for the -5/3 slope at the small-scale end (Sun et al. 2017; Durran and Weyn 2016). Moist physics have also been shown to be the key for the upscale error propagation (Zhang et al. 2003, 2007; Selz and Craig 2015). Hence, moist convection might be the actual source for both the shallower kinetic energy spectrum and the intrinsic predictability limit. If that is the case, slightly perturbing the moist physics scheme or the location of the convective grid will also lead to similar intrinsic predictability limit and error growth processes even in a coarse resolution model that is unable to

Accepted for publication in *Journal of the Atmospheric Sciences*. DOI 10.1175/JAS-D-19-0271.1.

resolve the transition of the slope (e.g., Tribbia and Baumhefner 2004). Ongoing research is being done to study the underlying physical processes for error growth behavior and will be reported separately in the future.

Another limitation of this hybrid framework is the lack of vertical structure in the model. Studies have shown that there is some degree of height dependence in the observed and simulated atmospheric spectra (Judt 2018). More critical differences may be found between the troposphere and the stratosphere (Skamarock et al. 2014). Given the connection between the background kinetic energy spectrum and the error growth behavior, it is very likely that differences in the spectrum could be associated with different predictability limits in the stratosphere and the troposphere. Their coupling will add another layer of complexity to the study (Butler et al. 2019).

With all these inadequacies aside, the most promising and encouraging finding of this study is that this simple new theoretical framework, which is built and based on the hybrid kinetic energy spectrum, could capture the error growth behavior found in the complex full-physics simulation. This strong connection between the kinetic energy spectrum and the error growth process might also apply to other turbulent fluids, like the ocean, which is less understood now. Our simple model may provide a new perspective for the predictability of these turbulent fluids and beyond, as will be further examined in future studies.

Accepted for publication in *Journal of the Atmospheric Sciences*. DOI 10.1175/JAS-D-19-0271.1.

Appendix A

Hybrid Model details

The derivation of Eq. (2) can be found in detail in L69 and RS2008 and hence will not be repeated here. It is assumed that all motions may adequately be represented by a relatively short sequence of spectral bands (*1, 2, ..., n*), with corresponding nondimensional wavenumber $N_1, N_2, \ldots, N_n$. Adjacent spectral bands are differed by a resolution factor ρ, so that $N_K = \rho N_{K-1}$. Following L69 and RS2008, $C_{K,L}$ in Eq. (2) is shown to be

$$C_{K,L} = \sum_{m=1}^{n} B_{K-m,L-m}\, N_m^2\, X_m \qquad (A1)$$

where $B_{K,L}$ is derived to represent the triads interaction between the spectral bands (*K, L*). X_m is basic-state kinetic energy integrated over the *m*th spectral band. If the kinetic energy spectrum $E(k) \sim k^{-p}$, then it is easy to show that $X_m \sim \rho^{-m(p-1)}$, following the definition of L69. Hence the impact of basic-state kinetic energy spectrum on error growth is primarily through X_m, whereas different dynamical formulation (SQG or 2DV) would lead to different $B_{K,L}$. The results of RS2008 have shown that X_m is the dominant factor in determining $C_{K,L}$ and error growth behavior.

In L69 and RS2008, the derivation and calculation of $C_{K,L}$ in Eq. (A1) are both based on a kinetic energy spectrum that processes one constant slope only (-3 or -5/3). To form our consistent hybrid framework, we assume the observed hybrid spectrum can be represented by two separate segments,

$$X_m = X_m^{2DV} + X_m^{SQG} \qquad (A2)$$

therefore $C_{K,L}^{2DV}$ and $C_{K,L}^{SQG}$ can be calculated according to X_m^{2DV} and X_m^{SQG}, respectively. The amplitude of X_m^{2DV} and X_m^{SQG} is set so that $X_m^{2DV} = X_m^{SQG}$ at transitional spectral band *m*. Moreover,

Accepted for publication in *Journal of the Atmospheric Sciences*. DOI 10.1175/JAS-D-19-0271.1.

493 for the convenience of dimensional analysis, the total energy $\sum_{m=1}^{n} X_m$ is set to be 1. As is shown
494 in RS2008, computation of $B_{K,L}$ get increasingly difficult when $K = L$ and they are both large,
495 due to rapidly decreasing integration area. In this study, a total of 24 spectral bands are used
496 whereas resolution factor ρ is set to $\sqrt{2}$, which means the smallest scale is ~10km after
497 dimensional results.

498 Note we could also compute a single matrix C and hence form an L69-type system of ODEs
499 based on the hybrid spectrum in (A2) under 2DV dynamics (as done in Durran and Gingrich 2014),
500 utilizing the fact that −5/3 is also an admissible spectral slope for 2DV if we add small-scale
501 forcing. However, we believe this single matrix assumption is as unphysical as our current
502 approach, if not more. If we examine the derivation process for matrix C in L69, the "inertial
503 range" idea is implicitly adopted, where no energy source/sink is considered during the derivation.
504 Under this "inertial range" idea, it is unlikely for the 2DV system itself to present a hybrid spectrum
505 automatically. It is also unphysical to assume the small-scale motions still obey the 2DV dynamics.
506 Therefore, we choose our current approach in the manuscript, which keeps the consistency
507 between the "inertial range" assumption and the derivation of $C_{K,L}$ terms for different systems.
508 Nonetheless, this should have a minor effect on our results given the results shown in earlier studies
509 (RS2008; Durran and Gingrich 2014)

510 The nonlinearity saturation effect introduced by Durran and Gingrich (2014) is also
511 included in our study. The original set of *n* second-order differential equations in Eq. (2) can be
512 rewritten to a set of *2n* first-order differential equations.

513 $$\frac{dZ_K}{dt} = Y_K \ , \quad \frac{dY_K}{dt} = \sum_{L=1}^{n} C_{K,L} Z_L \qquad (A3)$$

Accepted for publication in *Journal of the Atmospheric Sciences*. DOI 10.1175/JAS-D-19-0271.1.

An additional saturation term is added to the first equation in (A3) to force the error growth rate smoothly approaches to zero. Hence the system in (A3) becomes

$$\frac{dZ_K}{dt} = \left(1 - \frac{Z_K}{X_K}\right) Y_K \ , \quad \frac{dY_K}{dt} = \sum_{L=1}^{n} C_{K,L} Z_L \qquad (A4)$$

These first-order differential equations are the final system we solve numerically. Also, since the solution will asymptotically approach its saturation value under Durran and Gingrich (2014) adjustment, we define the saturation time as the time when Z_K/X_K equal 99% in the numerical solution.

Appendix B

Upscale error cascade in a turbulent fluid

Following the classical homogeneous turbulence approach, an estimate of the time needed for the small-scale error to contaminate the entire system can be derived as follows. Assume errors on a small scale will most contaminate the motion at the next larger scale (e.g., adjacent spectral waveband in our study) in a time scale comparable to the eddy turnover time at that scale $\tau(k)$, defined by

$$\tau(k) \sim [v(k)k]^{-1} = [E(k)k^3]^{-\frac{1}{2}} \qquad (B1)$$

Where k is the horizontal wavenumber, $v(k)$ is the velocity at this horizontal scale, and $E(k)$ is the background kinetic energy spectrum. More generally, errors initially confined to a relatively small scale (wavenumber $2k$) will contaminate a larger scale (wavenumber k) after time $\tau(k)$ in Eq. B1. In other words, the time needed for the error to propagate per unit wavenumber is $\frac{\tau(k)}{k}$. Thus, the total time needed for errors to propagate from the small scale k_s to the large scale k_l could then be estimated as

Accepted for publication in *Journal of the Atmospheric Sciences*. DOI 10.1175/JAS-D-19-0271.1.

$$T \sim \int_{k_l}^{k_s} \frac{\tau(k)}{k} dk = \int_{k_l}^{k_s} \frac{[E(k)k^3]^{-\frac{1}{2}}}{k} dk \qquad (B2)$$

Assume the kinetic energy spectrum of the background flow satisfy the power-law form $E \sim Ak^{-p}$, We have,

$$T \sim \begin{cases} A^{-\frac{1}{2}} ln\left(\frac{k_s}{k_l}\right), & p = 3 \\ \frac{2}{A^{\frac{1}{2}}(p-3)}\left(k_s{}^{\frac{(p-3)}{2}} - k_l{}^{\frac{(p-3)}{2}}\right), & p \neq 3 \end{cases} \qquad (B3)$$

If we can reduce our initial error to smaller and smaller scales, then in the limit of $k_s \to \infty$,

$$T \sim \begin{cases} \infty, & p \geq 3 \\ \frac{2}{(3-p)}\left[Ak_l{}^{(-p+3)}\right]^{-\frac{1}{2}} \sim \tau(k_l), & p < 3 \end{cases} \qquad (B4)$$

Thus T (the predictability limit), the time needed for errors at the smallest scales propagate to the largest scale, will grow larger and larger for a turbulent system with a steep slope $p \geq 3$. However, for $p < 3$, predictability time remains finite no matter how we confine the initial error. And this finite predictability time has the same order of magnitude as the eddy turnover time at the largest scale k_l.

Accepted for publication in *Journal of the Atmospheric Sciences*. DOI 10.1175/JAS-D-19-0271.1.

548 **Acknowledgment:**

549 Y. Qiang Sun is funded under award NA18OAR4320123 from the National Oceanic and
550 Atmospheric Administration, U. S. Department of Commerce. Fuqing Zhang is supported by NSF
551 Grants AGS-1305798 and 1712290, and ONR Grant N000140910526. Computing is performed at
552 ECMWF and the Texas Advanced Computer Center. The authors thank Richard Rotunno for
553 providing original code for their model. Discussions with Linus Magnusson and many other
554 researchers on related subjects are beneficial**.**

555

Accepted for publication in *Journal of the Atmospheric Sciences*. DOI 10.1175/JAS-D-19-0271.1.

References

Alley, R. B., K. Emanuel, and F. Zhang, 2019: Advances in Weather Prediction. *Science*, **363**, 342-344.

Bauer, P., A. Thorpe, and G. Brunet, 2015: The quiet revolution of numerical weather prediction. *Nature*, **525**, 47–55.

Bierdel, L., Selz, T. and Craig, G.C., 2018: Theoretical aspects of upscale error growth on the mesoscales: Idealised numerical simulations. *Q. J. Roy. Meteor. Soc*., **144,** 682-694, doi:10.1002/qj.3236

Butler, A., Charlton- Perez, A., Domeisen, D. I. V., Garfinkel, C., Gerber, E. P., Hitchcock, P., Karpechko, A. Y., Maycock, A. C., Sigmond, M., Simpson, I., & Son, S.- W. (2019). Sub-seasonal predictability and the stratosphere. In *Sub- seasonal to seasonal prediction* (pp. 223–241). B.V.: Elsevier.

Callies, J., R. Ferrari, and O. Bühler, 2014: Transition from geostrophic turbulence to inertia–gravity waves in the atmospheric energy spectrum. *Proc. Natl. Acad. Sci. USA*, **111**, 17 033–17 038, doi:https://doi.org/10.1073/pnas.1410772111.

Charney, J. G., 1971: Geostrophic turbulence. *J. Atmos. Sci.*, **28**, 1087–1095, doi:https://doi.org/10.1175/1520-0469(1971)028<1087:GT>2.0.CO;2.

Dalcher, A. and E. Kalnay, 1987: Error growth and predictability in operational ECMWF forecasts. *Tellus*, **39**, 474-491.

Daley, R., 1981: Predictability experiments with a baroclinic model. *Atmos.–Ocean*, **19,** 77–89.

Durran, D.R. and M.A. Gingrich, 2014: Atmospheric Predictability: Why Butterflies Are Not of Practical Importance. *J. Atmos. Sci.,* **71,** 2476-2488

Accepted for publication in *Journal of the Atmospheric Sciences*. DOI 10.1175/JAS-D-19-0271.1.

578 Durran, D.R., and J.A. Weyn, 2016: Thunderstorms don't get butterflies. *Bull. Amer. Meteor. Soc.*,
579 **97,** 237-243

580 Froude, L. S. R., L. Bengtsson, and K. I. Hodges, 2013: Atmospheric predictability revisited.
581 *Tellus*, **65**, 19022, https://doi.org/10.3402/tellusa.v65i0.19022.

582 Held, I. M., R. T. Pierrehumbert, S. T. Garner, and K. L. Swanson, 1995: Surface quasi-geostrophic
583 dynamics. *J. Fluid Mech.*, **282,** 1–20.

584 Herrera, M. A., I. Szunyogh, and J. Tribbia, 2016: Forecast uncertainty dynamics in the
585 THORPEX Interactive Grand Global Ensemble (TIGGE). *Mon. Wea. Rev.*, **144**, 2739–2766.

586 Judt, F., 2018: Insights into atmospheric predictability through global convection-permitting
587 model simulations. *J. Atmos. Sci.*, **75**, 1477–1497.

588 Judt, F., 2020: Atmospheric Predictability of the Tropics, Middle Latitudes, and Polar Regions
589 Explored through Global Storm-Resolving Simulations. *J. Atmos. Sci*., **77**, 257–276.

590 Kraichnan, R. H., 1967: Inertial ranges in two-dimensional turbulence. *Phys. Fluids*, **10**, 1417–
591 1423.

592 Leith, C. E., and R. H. Kraichnan, 1972: Predictability of turbulent flows. *J. Atmos. Sci.*, **29,** 1041–
593 1052.

594 Lindborg, E., 1999: Can the atmospheric kinetic energy spectrum be explained by two-
595 dimensional turbulence? *J. Fluid Mech.*, **388**, 259–288.

596 Lorenz, E. N., 1969: Predictability of a flow which possesses many scales of motion. *Tellus*, **21,**
597 289–307.

Accepted for publication in *Journal of the Atmospheric Sciences*. DOI 10.1175/JAS-D-19-0271.1.

598 Lorenz, E. N., 1973: On the existence of extended range predictability. *J. Appl. Meteor*.,**12**, 543–
599 546

600 Lorenz, E. N., 1982: Atmospheric predictability experiments with a large numerical model. *Tellus*,
601 **34**, 505–513, https://doi.org/10.3402/tellusa.v34i6.10836.

602 Lorenz, E. N., 1984: Estimates of atmospheric predictability in the medium range. *Predictability*
603 *of Fluid Motions: A.I.P. Conference Proceedings*, No. **106**, American Institute of Physics, La
604 Jolla Institute, 133–140.

605 Magnusson, L., and E. Källén, 2013: Factors influencing skill improvements in the ECMWF
606 forecasting system. *Mon. Wea. Rev.*, **141**, 3142–3153.

607 Marenco, A., and Coauthors, 1998: Measurement of ozone and water vapor by Airbus in-service
608 aircraft: The MOZAIC airborne program, an overview. *J. Geophys. Res.*, **103,** 25631–25642.

609 Nastrom, G., and K. Gage, 1985: A climatology of atmospheric wavenumber spectra of wind and
610 temperature observed by commercial aircraft. *J. Atmos. Sci.*, **42**, 950–960.

611 Palmer, T., A. Döring, and G. Seregin, 2014: The real butterfly effect. *Nonlinearity*, **27**, R123–
612 R141.

613 Reeves, R. W, 2014: Edward Lorenz revisiting the limits of predictability and their implications:
614 an interview from 2007. *Bull. Am. Meteor. Soc.* **95**, 681–687.

615 Rossby, C.-G., 1939: Relation between variations in the intensity of the zonal circulation of the
616 atmosphere and the displacements of the semi-permanent centers of action. *J. Mar. Res*., **2**,
617 38-55.

618 Rotunno, R., and C. Snyder, 2008: A generalization of Lorenz's model for the predictability of
619 flows with many scales of motion. *J. Atmos. Sci.*, **65**, 1063–1076.

Accepted for publication in *Journal of the Atmospheric Sciences*. DOI 10.1175/JAS-D-19-0271.1.

620 Selz, T., and G. C. Craig, 2015: Upscale error growth in a high-resolution simulation of a
621 summertime weather event over Europe. *Mon. Wea. Rev.*, **143**, 813–827,
622 doi:https://doi.org/10.1175/MWR-D-14-00140.1.

623 Skamarock, W. C., 2004: Evaluating mesoscale NWP models using kinetic energy spectra. *Mon.*
624 *Wea. Rev.*, **132**, 3019–3032, doi:https://doi.org/10.1175/MWR2830.1.

625 Skamarock, W. C., S.-H. Park, J. B. Klemp, and C. Snyder, 2014: Atmospheric kinetic energy
626 spectra from global high-resolution nonhydrostatic simulations. *J. Atmos. Sci.*, **71**, 4369–
627 4381, doi:https://doi.org/10.1175/JAS-D-14-0114.1.

628 Smagorinsky, J., 1969: Problems and promises of deterministic extended range forecasting. *Bull.*
629 *Amer. Meteor. Soc.*, **50**. 286–311.

630 Sun, Y. and F. Zhang, 2016: Intrinsic versus practical limits of atmospheric predictability and the
631 significance of the butterfly effect. *J. Atmos. Sci.*, **73**, 1419–1438.

632 Sun, Y. Q., R. Rotunno, and F. Zhang, 2017: Contributions of moist convection and internal
633 gravity waves to building the atmospheric −5/3 kinetic energy spectra. *J. Atmos. Sci.*, **74**, 185–
634 201, doi:https://doi.org/10.1175/JAS-D-16-0097.1.

635 Tribbia, J. J., and D. P. Baumhefner, 2004: Scale interactions and atmospheric predictability: An
636 updated perspective. *Mon. Wea. Rev.*, **132**, 703–713

637 Tulloch R, Smith KS, 2006: A theory for the atmospheric energy spectrum: Depth-limited
638 temperature anomalies at the tropopause. *Proc Natl Acad Sci USA*. **103**(40),14690–14694.

639 Vallis, G. K., 2006: *Atmospheric and Oceanic Fluid Dynamics*. Cambridge University Press, 745
640 pp.

Accepted for publication in *Journal of the Atmospheric Sciences*. DOI 10.1175/JAS-D-19-0271.1.

641 Waite, M. L., and C. Snyder, 2013: Mesoscale energy spectra of moist baroclinic waves. *J. Atmos.*
642 *Sci.*, **70**, 1242–1256

643 Žagar, N., M. Horvat, Ž. Zaplotnik, and L. Magnusson, 2017: Scale-dependent estimates of the
644 growth of forecast uncertainties in a global prediction system. *Tellus*, **69A**, 1287492,
645 https://doi.org/10.1080/16000870.2017.1287492.

646 Zhang, F., C. Snyder, and R. Rotunno, 2003: Effects of moist convection on mesoscale
647 predictability. *J. Atmos. Sci*. **60**, 1173-1185.

648 Zhang F., N. Bei, R. Rotunno, C. Snyder, C. C. Epifanio, 2007: Mesoscale predictability of moist
649 baroclinic waves: Convection-permitting experiments and multistage error growth dynamics.
650 *J. Atmos. Sci*. **64**, 3579–3594.

651 Zhang, F., Y.Q. Sun, L. Magnusson, R. Buizza, S.-J. Lin, J.-H. Chen and K. Emanuel, 2019: What
652 is the Predictability Limit of Midlatitude Weather? *J. Atmos. Sci*. **76**, 1077-1091.
653 doi:10.1175/JAS-D-18-0269.1
654

Accepted for publication in *Journal of the Atmospheric Sciences*. DOI 10.1175/JAS-D-19-0271.1.

Figure Legends

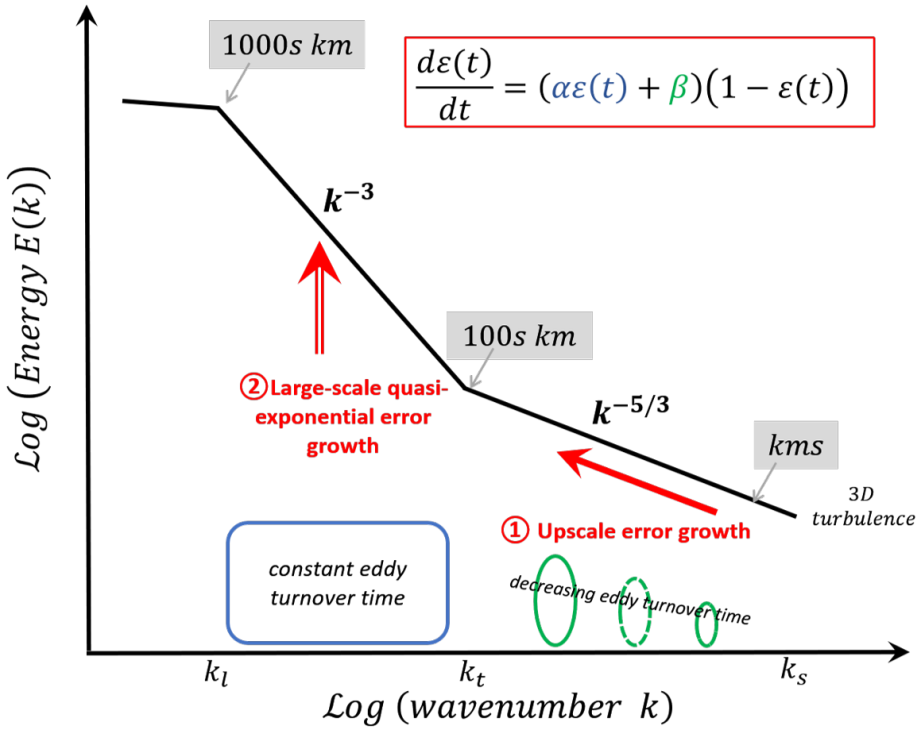

Figure 1. A schematic diagram for the canonical atmospheric kinetic energy spectrum (adopted from Skamarock et al. 2014) and illustration of our proposed two-stage error growth hypothesis: ① the initial small-amplitude error triggers error growth which saturates first at the smallest scales and subsequently propagates upscale at the wavelength range with a shallower -5/3 slope; and ② quasi-exponential error growth until saturation at synoptic scales in the wavelength range with a -3 slope. See details on the scales and equations in the text.

Accepted for publication in *Journal of the Atmospheric Sciences*. DOI 10.1175/JAS-D-19-0271.1.

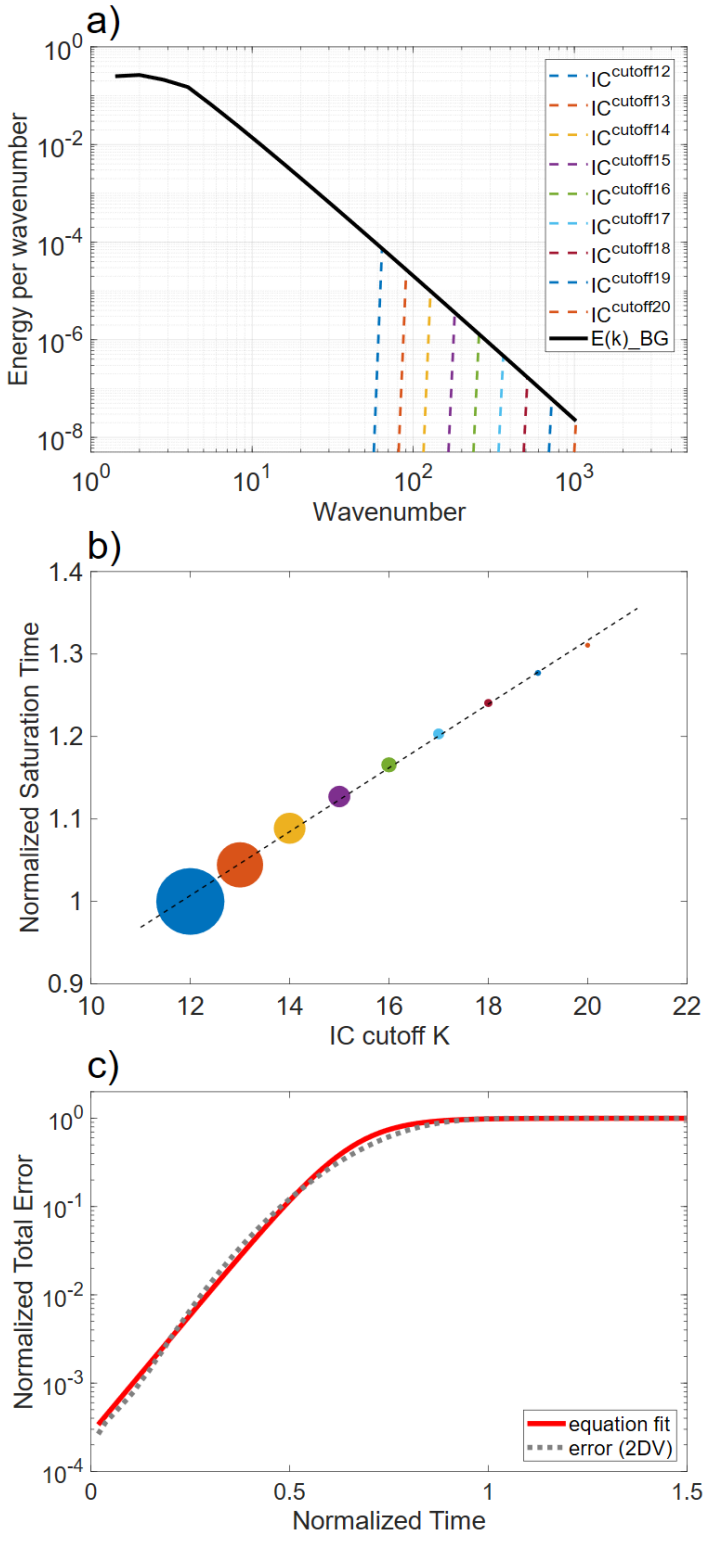

667

668 **Figure 2. Predictability limit for the 2DV case with a -3 slope.**

Accepted for publication in *Journal of the Atmospheric Sciences*. DOI 10.1175/JAS-D-19-0271.1.

669 **a)** Initial condition errors setup for our experiments, with the cutoff spectral band *K* increasing
670 from 12 to 20. **b)** corresponding normalized error saturation time at large scales (~5000km).
671 The size of the circle is symbolic of the amplitude of the initial condition error. The dashed line is
672 the linear fit of the results. **c)** comparison between numerically solved Eq. 2 (dash line) and fitted
673 results (red line) using Eq. 6 under 2DV dynamics.
674

Accepted for publication in *Journal of the Atmospheric Sciences*. DOI 10.1175/JAS-D-19-0271.1.

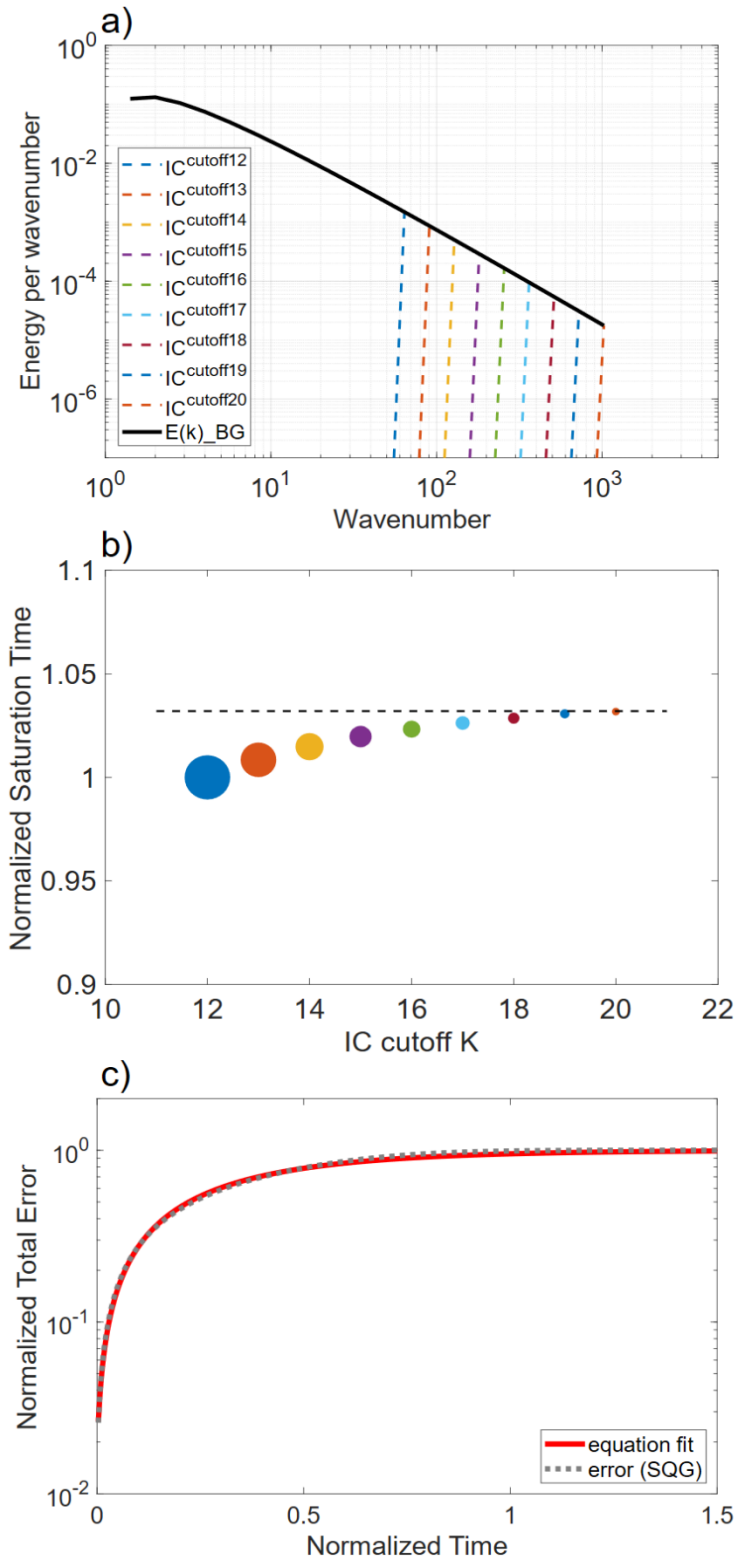

675

676 **Figure 3. Predictability limit for the SQG case with a -5/3 slope (otherwise the same as in Figure**

677 **2). a)** Initial condition errors setup for our experiments. **b)** corresponding normalized error

Accepted for publication in *Journal of the Atmospheric Sciences*. DOI 10.1175/JAS-D-19-0271.1.

678 saturation time at large scales (~5000km). With reduced initial condition error (increased IC
679 cutoff number), error saturation time in SQG approaches to a fixed value (dash line), and thus
680 predictability is intrinsically limited. **c)** comparison between numerically solved Eq. (2) (dash line)
681 and fitted results (red line) using Eq. (8) under SQG dynamics.
682

Accepted for publication in *Journal of the Atmospheric Sciences*. DOI 10.1175/JAS-D-19-0271.1.

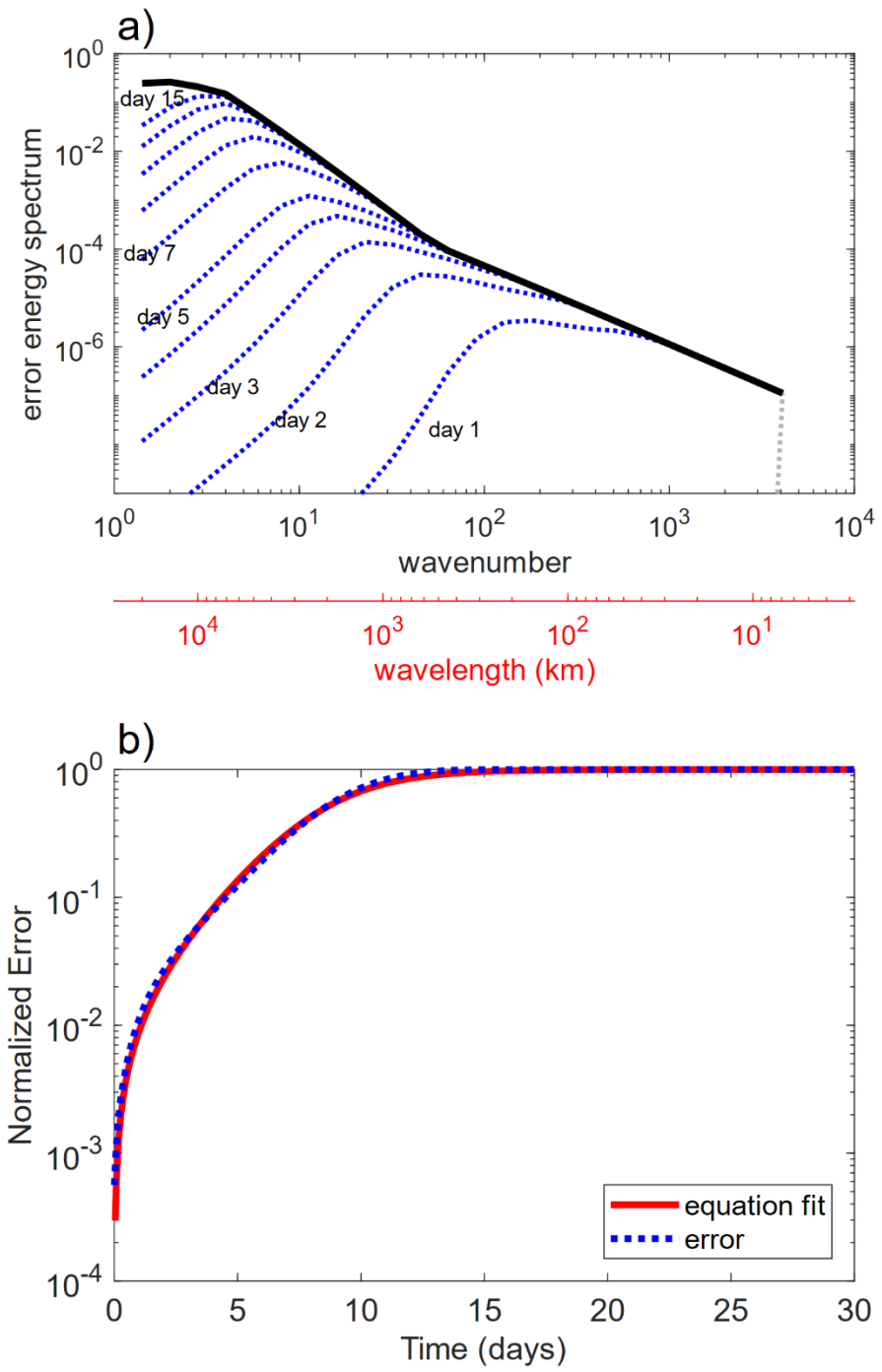

683

684 **Figure 4. Error evolution in our new hybrid-model framework.** **a)** error kinetic energy spectral

685 density (blue dash lines) as a function of wavenumber *k* at dimensional time t = 1, 2, 3, 4, 5, 7, 9,

686 11, 13, 15 days numerically solved from saturation-adjusted Eq. (9) along with the base state

687 background spectrum (black line). **b)** total error energy (blue dash line) integrated over all the

Accepted for publication in *Journal of the Atmospheric Sciences*. DOI 10.1175/JAS-D-19-0271.1.

spectral bands from the solution of saturation adjusted Eq. (9) versus the fitted total error evolution (red line) using our analytically derived error model (Eq. 14). The fitted $\alpha = 0.49\ day^{-1}, \frac{\beta}{\alpha} = 0.014$.

Accepted for publication in *Journal of the Atmospheric Sciences*. DOI 10.1175/JAS-D-19-0271.1.

692 **TABLE LIST**

693

694 **Table 1.** Range of predictability limits for different length scales calculated using the Lorenz-69

695 model versus our new, more realistic hybrid-model framework.

696

Length Scale	*Lorenz-69 Saturation time*	*Our hybrid model Saturation time*
10000 km	*5.6 days*	*19.2 days*
5000 km	*3.2 days*	*13.8 days*
2500 km	*1.8 days*	*10.4 days*
1250 km	*1.1 days*	*7.9 days*
625 km	*15.7 hours*	*5.5 days*
313 km	*9.5 hours*	*4.0 days*
156 km	*5.8 hours*	*2.8 days*
78 km	*3.6 hours*	*1.9 days*
39 km	*2.2 hours*	*1.2 days*

697

698

699

700

Accepted for publication in *Journal of the Atmospheric Sciences*. DOI 10.1175/JAS-D-19-0271.1.